Small particles in homogeneous turbulence: Settling velocity enhancement by two-way coupling

Thorsten Bosse[a] and Leonhard Kleiser
Institute of Fluid Dynamics, ETH Zürich, Zürich, Switzerland

Eckart Meiburg
Department of Mechanical and Environmental Engineering, University of California at Santa Barbara, Santa Barbara, California 93106

(Received 18 May 2005; accepted 6 December 2005; published online 6 February 2006)

The gravitational settling of an initially random suspension of small solid particles in homogeneous turbulence is investigated numerically. The simulations are based on a pseudospectral method to solve the fluid equations combined with a Lagrangian point-particle model for the particulate phase (Eulerian-Lagrangian approach). The focus is on the enhancement of the mean particle settling velocity in a turbulent carrier fluid, as compared to the settling velocity of a single particle in quiescent fluid. Results are presented for both one-way coupling, when the fluid flow is not affected by the presence of the particles, and two-way coupling, when the particles exert a feedback force on the fluid. The first case serves primarily for validation purposes. In the case with two-way coupling, it is shown that the effect of the particles on the carrier fluid involves an additional increase in their mean settling velocity compared to one-way coupling. The underlying physical mechanism is analyzed, revealing that the settling velocity enhancement depends on the particle loading, the Reynolds number, and the dimensionless Stokes settling velocity if the particle Stokes number is about unity. Also, for particle volume fractions $\Phi_v \gtrsim 10^{-5}$, a turbulence modification is observed. Furthermore, a direct comparison with recent experimental studies by Aliseda *et al.* [J. Fluid Mech. **468**, 77 (2002)] and Yang and Shy [J. Fluid Mech. **526**, 171 (2005)] is performed for a microscale Reynolds number $\mathrm{Re}_\lambda \approx 75$ of the turbulent carrier flow. © *2006 American Institute of Physics*. [DOI: 10.1063/1.2166456]

I. INTRODUCTION

Particle settling and sedimentation is central to all disperse two-phase flows in which the particle density is larger than the density of the carrier fluid. These flows include a variety of natural multiphase systems as well as engineering applications. Examples are dust particle transport in the atmosphere, particle sedimentation in river beds, or turbo inhaler devices for medical purposes.

In the past, numerical simulation studies of turbulent flows laden with particles focused primarily on particle dispersion, preferential concentration of particles, and turbulence modification of the carrier fluid (see, e.g., Squires and Eaton,[1] Elghobashi and Truesdell,[2] and the reviews by Eaton and Fessler[3] and Crowe *et al.*[4]). Usually, particle dispersion is dominated by the large-scale dynamics, for example in mixing layers (e.g., Wen *et al.*[5]) and wake flows (e.g., Tang *et al.*[6]). The preferential accumulation of particles, however, is mostly related to small-scale dynamics. In isotropic turbulence, heavy particles were shown to accumulate preferentially in regions of high strain rate and low vorticity (Squires and Eaton,[7] Wang and Maxey[15]). Here, the associated time scale is the Kolmogorov time and the characteristic length scale is typically an order of magnitude larger than the Kolmogorov length (Yang and Lei,[17] Yang and Shy[20]).

Squires and Eaton[8] were among the first to account for the particles' effect on the turbulence properties (two-way coupling) in their direct numerical simulations. They found an increase of the turbulent kinetic energy at high wave numbers relative to the energy at low wave numbers. In a number of subsequent investigations, turbulence modification was further examined, including the influence of different parameters such as the Stokes number or the particle loading on the fluid-particle interaction (e.g., Elghobashi and Truesdell,[9,10] Boivin *et al.*,[11] Druzhinin,[12] Ferrante, and Elghobashi,[13] and several more).

Despite these quite exhaustive studies of particle dispersion and turbulence modification by particles with and without gravity, there have been only a few investigations focusing on the mean particle settling rate in homogeneous turbulence. Maxey[14] studied particle settling in homogeneous turbulence and random flow fields revealing an increase in the mean particle settling velocity compared to the terminal velocity of a single particle in still fluid. In a direct numerical simulation of isotropic turbulence, Wang and Maxey[15] also found an increase of the mean settling velocity. They explained their findings as a consequence of the "preferential sweeping effect," by which the particles are swept preferably toward regions of downward fluid motion when encountering an eddy. Mei[16] studied the effect of turbulence on the particle settling velocity using a Monte Carlo method. Here, the focus was on the nonlinear particle drag range. In

[a]Author to whom all correspondence should be addressed. Electronic mail: bosse@ifd.mavt.ethz.ch

contrast to Wang and Maxey, Mei predicted that the mean particle settling velocity may become less than the velocity of a single particle in still fluid. Yang and Lei[17] performed direct numerical and large-eddy simulations of particles settling in homogeneous, isotropic turbulence. Their results are in good agreement with those by Wang and Maxey. However, both of these investigations were limited to dilute suspensions with small-particle volume fractions where the particles do not have any effect on the carrier flow (one-way coupling).

The available experimental studies of particle settling in homogeneous turbulence are quite limited. Aliseda *et al.*[18] measured the enhancement of the particle settling velocity in nearly homogeneous, isotropic turbulence for particle volume fractions up to $\Phi_v = 7 \times 10^{-5}$. They found significantly larger particle settling velocities than those computed by Wang and Maxey. Yang and Shy[19] investigated particle settling in aqueous near-isotropic turbulence generated by a pair of vibrating grids. The focus was on the nonlinear drag range with particle Reynolds numbers up to $\mathrm{Re}_p = 39$ and nondimensional terminal settling velocities of a single particle of $U_p/u_\eta = 5, \ldots, 30$. In this parameter range, Yang and Shy found a maximum of the settling velocity enhancement of about 7%. In a recent experiment, Yang and Shy[20] studied the particle settling rate and turbulence modification by heavy microparticles in near-isotropic turbulence generated by a pair of counter-rotating fans. For particle Reynolds numbers $\mathrm{Re}_p < 1$, they observed a mean particle settling velocity enhancement that is considerably smaller than that reported by Aliseda *et al.* and, thus, much closer to the numerical results by Wang and Maxey and Yang and Lei.

These contradicting findings and, in particular, the discrepancies between one-way coupled simulations and the experiments by Aliseda *et al.* call for a systematic numerical study of two-way coupling effects with respect to the mean particle settling velocity in homogeneous turbulence. This is the focus of the present paper. In the case of one-way coupling, the results by Wang and Maxey will be used for validation purposes. Two-way coupling will be shown to involve an additional enhancement of the settling velocity compared to one-way coupling for sufficiently large particle loadings. The underlying physical mechanism will be analyzed in detail for different particle volume fractions in the range $10^{-6} \leqslant \Phi_v < 10^{-3}$. Particle distribution characteristics, such as the correlation between vorticity and regions of particle accumulation, will be analyzed for both one-way and two-way coupling. Moreover, it will be shown that a modulation of the turbulent properties of the carrier flow by the particles sets in for volume fractions as low as $\Phi_v \approx 10^{-5}$. Although turbulence modulation is not the focus of this study, some changing turbulent properties of the carrier flow are examined, since these are directly linked to the enhancement of the particle settling velocity. Furthermore, a direct comparison with the experimental findings by Aliseda *et al.*[18] as well as Yang and Shy[20] will be performed by matching the simulation parameters as closely as possible to those in the experiments. This last step is primarily done in response to an obvious lack of close adjustments of experiments and simulations to the same set of parameters, which is generally observed in the available literature.

The paper is organized as follows. In Sec. II we present the governing equations, the numerical method to solve these equations, and the definitions of some turbulent quantities used in the analysis. Section III contains validation results regarding the implementation of the turbulence forcing scheme as well as one-way and two-way coupled particle-laden flows. Results for two-way coupling and the comparison with the experiments are presented in Sec. IV. Finally, a summary of our findings is given in Sec. V.

II. SIMULATION APPROACH

The numerical method employed to solve the governing equations is known as the Eulerian-Lagrangian approach for particulate flows. The fluid equations are solved in an Eulerian framework using a Fourier pseudospectral method, whereas the particles are individually tracked along their trajectories. The computational domain is a cube of side length $L = 2\pi$ with periodic boundaries. Statistically stationary homogeneous turbulence is generated by means of a forcing procedure according to Eswaran and Pope.[21] The governing equations and the numerical implementation are very similar to those described in Bosse *et al.*[22] Therefore, we confine ourselves here to a short outline of the numerical approach.

A. Governing equations

We consider a dilute particle suspension, in which the particle concentration is small enough for interparticle collisions to be neglected. Moreover, all the particles have equal properties, and they are assumed to be much smaller than the smallest relevant scales of the fluid motion. This allows for the particles to be modeled as point forces without resolving their finite size. The trajectory of a single particle is given by

$$\frac{dY_i(t)}{dt} = v_i(t), \tag{1}$$

where $Y_i(t)$ is the particle position, $v_i(t)$ the particle velocity, $Y_i(0) = Y_i^{(0)}$ its initial position, and $i = 1, 2, 3$ denotes the three spatial directions. The particle motion is governed by the equation derived by Maxey and Riley,[23] simplified for small heavy particles,

$$\frac{dv_i(t)}{dt} = \frac{1}{\tau_p}\{[u_i(\mathbf{Y}(t), t) - v_i(t)] - U_p \delta_{i3}\} \tag{2}$$

with the particle response time $\tau_p = m_p/(6\pi\mu r)$. Here, $u_i(\mathbf{Y}(t), t)$ indicates the fluid velocity at the instantaneous particle position, m_p the particle mass, μ the dynamic viscosity, and r the particle radius. The settling velocity of a single particle in still fluid, i.e., the Stokes velocity, is given by

$$U_p = \tau_p g \left(1 - \frac{\varrho}{\varrho_p}\right) \tag{3}$$

with g being the magnitude of the gravitational acceleration, ϱ the fluid density, and ϱ_p the particle density.

The fluid motion is governed by the continuity equation,

$$\frac{\partial u_i}{\partial x_i} = 0, \tag{4}$$

and the incompressible Navier-Stokes equation augmented by a source term representing the particles' feedback force,

$$\frac{\partial u_i}{\partial t} + u_m \frac{\partial u_i}{\partial x_m} = -\frac{1}{\varrho}\frac{\partial p}{\partial x_i} + \nu \frac{\partial^2 u_i}{\partial x_m \partial x_m} + \frac{1}{\varrho} f_i^{(p)} \tag{5}$$

with the two-way coupling term

$$f_i^{(p)}(\mathbf{x}) = -\frac{6\pi\mu r \varrho_p}{m_p} \sum_{j=1}^{n_p^r} [u_{i,j}(\mathbf{Y}_j) - v_{i,j}] \delta(x_i - Y_{i,j}). \tag{6}$$

Here, $\nu = \mu/\varrho$ is the kinematic viscosity, and n_p^r denotes the number of (real) particles. The Dirac δ function indicates that the feedback force of particle j is applied as a point force at the instantaneous particle position $Y_{i,j}(t)$.

B. Dimensionless parameters

In order to define the properties of a dilute suspension of particles settling in homogeneous turbulence under gravity, we need to specify eight physical quantities. The fluid is characterized by the dynamic viscosity μ and the density ϱ. A single spherical particle is characterized by two quantities, e.g., the particle mass m_p and the particle radius r. Alternatively, one or both of these two could be replaced by the particle density ϱ_p and the particle volume V_p. The gravitational acceleration is given by g. In addition, we have to specify two parameters characterizing the size and the velocity of typical eddies in the turbulent flow. In the case of homogeneous turbulence, these are usually taken to be the Taylor microscale λ and the root-mean-square (rms) velocity u', respectively. Finally, to define the particle loading we have to specify how many particles are introduced into a unit volume. According to the Buckingham Π theorem, five nondimensional parameters can be formed from these eight quantities, which fully define the physical situation.

The turbulent motion of the carrier fluid is usually characterized by the microscale Reynolds number

$$\mathrm{Re}_\lambda = \frac{u'\lambda}{\nu}. \tag{7}$$

The particle properties are described by two nondimensional parameters, the Stokes number and the dimensionless Stokes settling velocity. Since particles much smaller than the smallest relevant scales of the fluid motion are considered, it is reasonable to define the Stokes number as the ratio of the particle response time to the Kolmogorov time scale,

$$\mathrm{St}_\eta = \frac{\tau_p}{t_\eta}. \tag{8}$$

Accordingly, the dimensionless Stokes settling velocity is based on the Kolmogorov velocity scale u_η,

$$U_p^* = \frac{U_p}{u_\eta}. \tag{9}$$

For a given turbulence level (dissipation rate ε and viscosity ν) and fixed gravitational constant g (as in a real-world experiment), the dimensionless Stokes velocity is related to the Stokes number according to

$$\frac{U_p}{u_\eta} = \mathrm{St}_\eta \left(\frac{\nu}{\varepsilon^3}\right)^{1/4} g\left(1 - \frac{\varrho}{\varrho_p}\right) = \mathrm{St}_\eta \frac{t_\eta}{u_\eta} g\left(1 - \frac{\varrho}{\varrho_p}\right). \tag{10}$$

In simulations, however, these two parameters are often chosen independently of each other implying that the gravitational acceleration g is adjusted accordingly (see, e.g., Wang and Maxey[15]).

Finally, the particle loading of the fluid is specified by either the particle volume fraction,

$$\Phi_v = \frac{(4/3)\pi r^3 n_p^r}{L^3}, \tag{11}$$

or, alternatively, the particle mass loading,

$$\Phi_m = \Phi_v \frac{\varrho_p}{\varrho}. \tag{12}$$

The five dimensionless parameters sufficient to define the properties of particles settling in homogeneous turbulence are taken to be Re_λ, St_η, U_p^*, ϱ_p/ϱ, and Φ_v. From these, all other properties, such as the particle radius or the mass loading, can be derived. For clarity we will provide additional parameters such as the number of particles in some cases.

Another important parameter is the particle Reynolds number, which is based on the particle radius and the relative velocity between particle and surrounding fluid,

$$\mathrm{Re}_p = \frac{|u_i(\mathbf{Y}) - v_i| r}{\nu}. \tag{13}$$

For the equation of motion, Eq. (2), to be valid, Re_p is required to be less than unity (Maxey and Riley[23]). The particle Reynolds number was monitored throughout the simulations and found to comply with this constraint.

C. Numerical implementation

In order to solve the governing fluid equations, a Fourier pseudospectral method was employed (see, e.g,. Orszag[24]). Each term in Eq. (5) was Fourier-transformed. The resulting ordinary differential equation was discretized and numerically solved in Fourier space using a combined Runge-Kutta/Crank-Nicolson scheme. The same scheme was applied for the time integration of the particle equations, Eqs. (1) and (2), in real space. The computational cube was discretized by a mesh of N equidistant grid points in each spatial direction x_i, and gravity was applied in the negative x_3 direction.

Unless otherwise mentioned, trilinear interpolation was used to compute both the Stokes drag term in the particle equation and the feedback forces of the particles at the grid points of the computational mesh. In order to estimate the influence of interpolation on the accuracy of our results, especially for the comparison with the experimental data, higher-order interpolation, i.e., third-order Lagrangian polynomials or spectral summation, was employed in some cases (cf. Sec. IV B).

In order to keep the computational effort at a reasonable cost, the point-particle approximation was augmented by introducing computational particles. Each computational particle served as a representative of M real particles ($M=n_p^r/n_p^c$ with $M\geqslant 1$). With the concept of computational particles included, the numerical algorithm described above changes only slightly, such that the right-hand side of Eq. (6) is multiplied by M and the sum is evaluated over all computational particles n_p^c rather than all real particles n_p^r. For a more detailed discussion of computational particles, the reader is referred to Elghobashi[25] or Druzhinin.[12]

At the beginning of a simulation, the particles were randomly distributed within the computational box and their initial velocity was set to the Stokes settling velocity. The turbulent motion of the fluid was generated and kept statistically stationary by the forcing procedure developed by Eswaran and Pope.[21] In this forcing procedure, energy is artificially added to the velocity components in Fourier space within a band of small wave numbers, $0\leqslant|k|\leqslant K_F$. The energy input is accomplished by an additional acceleration term in the Fourier-transformed Navier-Stokes equations, which is based on Ornstein-Uhlenbeck processes. To obtain desired turbulence properties, such as a specific microscale Reynolds number Re_λ, the forcing parameters have to be chosen appropriately. Unless otherwise indicated, the parameters $\varepsilon^*=16.997$, $T_L=0.038$, and $K_F=2\sqrt{2}$ were kept fixed, and only the forcing Reynolds number Re^* was adjusted to obtain different turbulence intensities (see Eswaran and Pope[21] for the definitions of the forcing parameters and implementation details).

In each time step, the mean fluid velocity in each direction was set to zero. In the x_3 direction this is equivalent to superposing a positive uniform pressure gradient that balances the net weight of the particles per unit volume (Maxey and Patel[26]). Since the computational domain contains no solid boundaries, this is necessary to keep the particles and the fluid from ever more accelerating in the negative x_3 direction due to gravity.

D. Turbulent quantities

In the literature, different definitions are available for various statistical quantities describing the turbulent flow properties. Therefore, it is necessary to state some of the definitions used in this study.

The turbulent kinetic energy is given by

$$q=\frac{1}{2}\langle u_i u_i\rangle=\int_0^\infty E(k)dk \tag{14}$$

with u_i being the velocity fluctuations, $k=|\mathbf{k}|$ the magnitude of a wave-number vector, and $E(k)$ the three-dimensional energy spectrum. The angle brackets indicate an ensemble average. Assuming homogeneous and isotropic conditions, this is equivalent to a spatial average. The energy content associated with shells of radius k in Fourier space is computed as

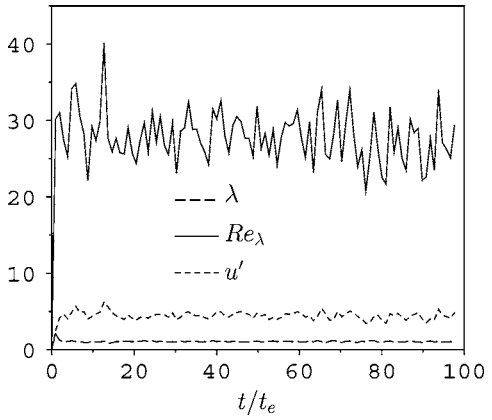

FIG. 1. Validation run f28, Eswaran and Pope (Ref. 21). Time evolution of Taylor microscale λ, microscale Reynolds number Re_λ, and rms velocity u'. $\bar{\lambda}=1.07$, $\bar{\mathrm{Re}}_\lambda=28.0$, $\overline{u'}=4.46$.

$$E(k)=\sum_{|\mathbf{k}|\in[k,k+dk]}\frac{|\hat{\mathbf{u}}(\mathbf{k},t)|^2}{2}, \tag{15}$$

where $\hat{\mathbf{u}}(\mathbf{k},t)$ is the Fourier coefficient of the velocity associated with wave number $\mathbf{k}$. The turbulent kinetic energy can be split into three fractions according to the three velocity components. For example, in the x_1 direction we have $q_1=0.5\langle u_1^2\rangle$, such that $q=q_1+q_2+q_3=3q_1=3q_2=3q_3$. Here, the last three equalities only hold in perfectly isotropic turbulence. In numerical simulations, the energy content will usually be slightly different in different spatial directions.

The dissipation rate is defined as

$$\varepsilon=\nu\left\langle\frac{\partial u_i}{\partial x_j}\frac{\partial u_i}{\partial x_j}\right\rangle=\int_0^\infty D(k)dk=\int_0^\infty 2\nu k^2E(k)dk \tag{16}$$

with $D(k)$ being the three-dimensional dissipation spectrum. Using ε, the Taylor microscale λ can be computed in homogeneous, isotropic turbulence according to

$$\lambda=\sqrt{15\nu\frac{u'^2}{\varepsilon}}. \tag{17}$$

Large eddies are characterized by the eddy length scale l_e, the velocity scale u', and the eddy turnover time t_e. The rms velocity is defined as

$$u'=\left(\frac{1}{3}\langle u_i'u_i'\rangle\right)^{1/2}=\sqrt{\frac{2}{3}q}. \tag{18}$$

The eddy length scale is defined as $l_e=u'^3/\varepsilon$, and the eddy turnover time is then given by $t_e=l_e/u'=u'^2/\varepsilon$. As an alternative way to characterize large-scale motion, the integral length scale l_I is obtained from the three-dimensional energy spectrum,

$$l_I=\frac{\pi}{2u'^2}\int_0^\infty\frac{E(k)}{k}dk. \tag{19}$$

Accordingly, the integral time scale is $t_I=l_I/u'$.

TABLE I. Comparison of nondimensional time-averaged turbulent quantities with runs f28 and f19 of Eswaran and Pope (Ref. 21).

	run	N	$k_0\eta$	$k_{\max}\eta$	$k_0 l_e$	Re_λ	t_e	ε
ESPO	f28	32	0.103	1.55	1.81	28.2	0.409	43.1
Present			0.103	1.55	1.77	28.0	0.406	45.3
ESPO	f19	64	0.045	1.36	1.18	42.2	0.138	382.9
Present			0.046	1.42	1.08	39.5	0.198	373.1

III. VALIDATION

In order to validate the implementation of the turbulence forcing scheme, two test simulations of homogeneous, isotropic turbulence without particles were performed with parameters given in the paper of Eswaran and Pope:[21] run f19 for $T_L=0$ and run f28 for $T_L\neq 0$. Figure 1 shows the time evolution of some turbulent quantities for run f28. Since the forcing starts with a zero velocity field, it takes a few eddy turnover times to "build up" the turbulence. Time-averaging was started after about 20 eddy turnover times ($20t_e$). All the quantities shown experience fluctuations over time. Their time average, however, remains stationary for $t\gtrsim 20t_e$. Thus, the forcing well accomplishes its primary task of maintaining stationary turbulence.

Table I provides a quantitative comparison of some computed turbulent quantities with those given in Table II of Eswaran and Pope.[21] It is important to note that the latter applied a "smoothing" procedure to their three–dimensional (3D) energy spectrum, from which other turbulent quantities were then derived. To obtain a 3D energy spectrum, the wave-number space is divided into a number of shells with increasing radii (see, e.g., Tennekes and Lumley[27]). The energy associated with all wave-number vectors of magnitude k is combined to give the energy content $E(k)$ of the shell with radius k [see also Eq. (15)]. Applying this procedure to a finite number of discrete wave-number vectors as done in numerical simulations leads to certain shells being under- or over-represented compared to a continuous wave-number space. This is taken into account by the smoothing procedure, which was also applied in our simulations to obtain the values shown in Table I. Good agreement of our results (present) with those by Eswaran and Pope[21] (ESPO) is found. Note that in all simulations presented in the following, smoothing was *not* applied to the energy spectra.

In the case of one-way coupling, the study of Wang and Maxey[15] (hereafter referred to as WM) is used for comparison and validation. The grid resolutions and corresponding forcing parameters were taken from Table I in WM to allow

TABLE II. Turbulent flow and particle quantities of simulations shown in Fig. 8. Two-way coupled simulations (runs No. 1–7) were started from a fully turbulent flow field with one-way coupled particles. In all simulations: $\varrho_p/\varrho=5000$, $n_p^c=100\,096$, forcing parameters $\varepsilon^*=0.01$, $T_L=0$, $K_F=2\sqrt{2}$, $\mathrm{Re}^*=8.58$. Last column shows the maximum difference between two-way and one-way coupling (run No. 0).

	One-way	Two-way							Max. Δ
Run No.	0	1	2	3	4	5	6	7	[%]
$\Phi_v/10^{-5}$	<0.1	0.15	1.5	3.0	4.5	7.0	9.0	15.0	
M	1	1	3.34	6.67	10.01	15.57	20.02	33.37	
Re_λ	42.70	42.56	41.69	39.90	37.04	33.61	30.75	24.50	42.6
λ	0.595	0.596	0.606	0.608	0.591	0.554	0.522	0.435	26.9
u'	8.42	8.32	8.02	7.69	7.37	7.11	6.90	6.56	22.1
q	105.5	103.5	96.2	88.0	80.6	75.2	70.9	64.4	38.8
q_1	102.5	102.4	92.4	88.0	77.2	67.5	61.8	48.8	52.4
q_2	105.5	103.4	93.9	84.9	76.4	69.0	61.8	48.4	54.1
q_3	108.2	104.6	102.3	96.2	88.2	89.0	88.9	95.8	18.5
ε	354.0	342.0	307.5	282.5	275.7	290.1	308.1	397.8	22.1
η	0.0465	0.0465	0.0478	0.0492	0.0497	0.0488	0.0481	0.0448	6.9
u_η	2.549	2.528	2.452	2.410	2.402	2.426	2.463	2.616	2.6
t_η	0.0184	0.0186	0.0196	0.0206	0.0210	0.0204	0.0197	0.0172	14.1
l_e	1.678	1.686	1.678	1.603	1.441	1.230	1.060	0.709	57.7
t_e	0.201	0.204	0.210	0.210	0.198	0.175	0.155	0.108	46.3
l_I	1.168	1.172	1.182	1.195	1.198	1.203	1.196	1.144	3.0
t_I	0.140	0.142	0.148	0.157	0.165	0.171	0.175	0.175	25.0
St_η	1.0	0.99	0.94	0.88	0.88	0.92	0.92	1.08	12.0
U_p/u_η	1.0	1.0	1.04	1.05	1.06	1.05	1.03	0.97	6.0
$\Delta V_3/U_p$	0.355	0.366	0.558	0.801	0.938	1.091	1.171	1.378	288
$\Delta V_3/u'$	0.107	0.112	0.177	0.264	0.323	0.390	0.431	0.534	399

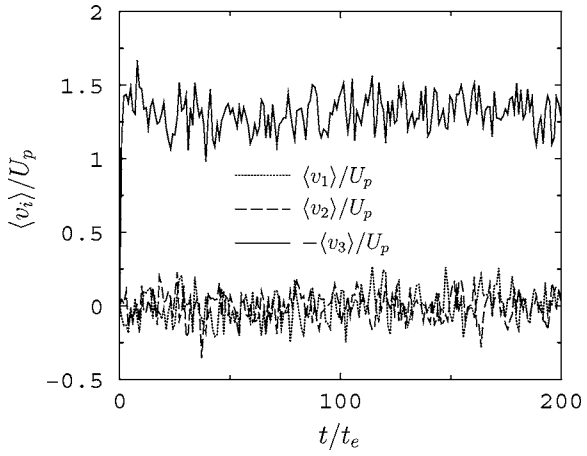

FIG. 2. Mean particle velocities $\langle v_i \rangle$ normalized by the Stokes settling velocity U_p as a function of time. $\mathrm{Re}_\lambda = 31$, $\mathrm{St}_\eta = 1$, $U_p/u_\eta = 1$, $N = 48$.

for a direct comparison of the results. The density ratio was $\varrho_p/\varrho = 1000$ in all simulations.

Figure 2 shows the time evolution of the mean particle velocities in the simulation with $N = 48$, $\mathrm{Re}_\lambda = 31$, $\mathrm{St}_\eta = 1$, and $U_p/u_\eta = 1$. Due to their initial velocity, the particles experience an immediate increase in settling velocity. After a transient period of about 50 eddy turnover times, the time average of the settling velocity converges to a statistically stationary value of about 1.3 times the Stokes settling velocity.

The settling velocity increase is defined here with respect to the Stokes settling velocity of a single particle as

$$\Delta V_3 := -\overline{\langle v_3 \rangle} - U_p, \tag{20}$$

where the angle brackets $\langle \cdot \rangle$ indicate an ensemble average over all particles at a certain point in time, and the overbar $\overline{\langle \cdot \rangle}$ denotes an additional time average. Figure 3 displays the relative increase in the mean settling velocity of particles for different particle Stokes numbers. The velocity enhancement is most pronounced for Stokes numbers around unity, i.e., when the particle response time is of the order of the Kolmogorov time scale. In the case of very small Stokes numbers, the particle inertia becomes negligible and the particles respond almost immediately to changes in the velocity of their fluid neighborhood. Hence, there is no significant particle accumulation and the preferential sweeping has a negligible effect. As a result, the mean settling velocity is about the same as that of a single particle in quiescent fluid. If the Stokes number is increased beyond unity, preferential sweeping is also less pronounced, in this case due to an increased particle inertia. These findings are in very good accordance with the results by WM. In the case of $\mathrm{Re}_\lambda = 21$ ($N = 32$), the velocity enhancement found in our simulations is slightly higher for Stokes numbers larger than unity, and slightly smaller for Stokes numbers below unity compared to WM. We also found a weak dependence on the microscale Reynolds number (only done for $\mathrm{St}_\eta = 1$, $\mathrm{Re}_\lambda = 31$, $\mathrm{Re}_\lambda = 43$), however, it is less pronounced than that reported by WM. It should be noted that in the case of $\mathrm{Re}_\lambda = 31$ ($N = 48$), WM also used a different turbulence forcing scheme for comparison, yielding the same qualitative features but quantitative differences of up to about 30%. Thus, differences in the results may be related to a slightly different implementation of the forcing procedure and/or the solution algorithm. Also, WM applied time averages over only a few eddy turnover times, whereas in our simulation the sampling period was of the order of 100 eddy turnover times.

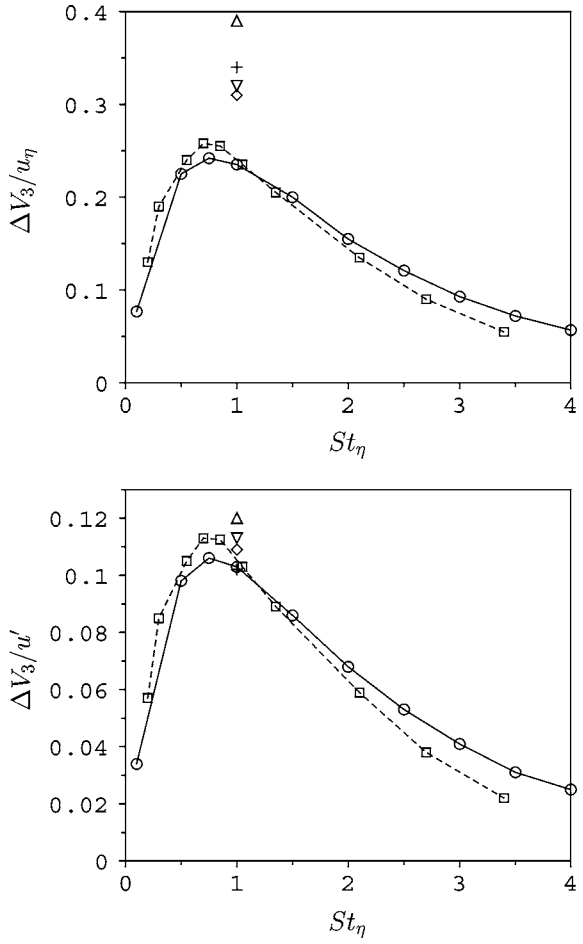

FIG. 3. Increase in the mean particle settling velocity as a function of the Stokes number. The velocity enhancement is normalized by the Kolmogorov velocity scale u_η (top) or the rms velocity scale u' (bottom). $\mathrm{Re}_\lambda = 21$ ($N = 32$): □ WM, ○ present work (solid and dashed lines). $\mathrm{Re}_\lambda = 31$ ($N = 48$): ▽ WM, ◇ present work. $\mathrm{Re}_\lambda = 43$ ($N = 64$): △ WM, + present work.

To quantify the preferential concentration of the particles, we consider the probability function $P_c(n_p^b)$ introduced by WM. The local particle volume fraction is denoted by Φ_v^l and computed by dividing the computational domain into N_b small boxes. The volume of such a box is equal to the grid cell volume and the box center coincides with a grid point ($N_b = N^3$). The function $P_c(n_p^b)$ specifies the probability of finding a certain number of particles n_p^b, i.e., a certain volume fraction or concentration, within a box. Following WM, we distinguish between four discrete events of finding zero, one, two, or more than two particles in a box. Given the relatively small number of particles compared to the number of boxes, this is a reasonable choice. For example, in the simulation with $\mathrm{Re}_\lambda = 31$ ($N = 48$) the number of particles was $n_p^r = n_p^c = 147456$, which is an average of 1.3 particles per box or grid cell. As the particles accumulate, the highest particle volume

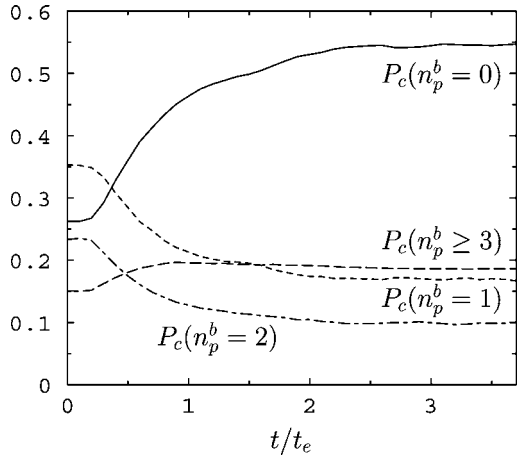

FIG. 4. Time evolution of the probability functions describing the likelihood of finding a certain number of particles n_p^b in a grid cell. $\mathrm{Re}_\lambda = 31$, $N = 48$, $\mathrm{St}_\eta = 1$, $U_p/u_\eta = 1$, one-way coupling.

fractions involve about seven particles, the lowest zero particles per box.

At the beginning of a simulation, the particle distribution was uniformly random. In this case, the probability functions can be computed exactly from the binomial distribution

$$P_{\mathrm{binom}}(n_p^b) = \binom{n_p^r}{n_p^b}\left(\frac{1}{N_b}\right)^{n_p^b}\left(1 - \frac{1}{N_b}\right)^{n_p^r - n_p^b}, \tag{21}$$

resulting in

$$P_{\mathrm{binom}}(n_p^b = 0) = 0.2636,$$

$$P_{\mathrm{binom}}(n_p^b = 1) = 0.3515,$$

$$P_{\mathrm{binom}}(n_p^b = 2) = 0.2343,$$

$$P_{\mathrm{binom}}(n_p^b \geqslant 3) = 0.1506.$$

These analytical values were reproduced in the simulation for the initial distribution at $t = 0$. The time evolution of the probability functions $P_c(n_p^b, t)$ is plotted in Fig. 4. Shortly after the particles are released, all functions start deviating from their initial value. The strongest increase is observed for $P_c(n_p^b = 0, t)$ reflecting large particle-free regions emerging from the initially uniform distribution. At the same time, regions of high particle volume fraction are growing as indicated by an increase of $P_c(n_p^b \geqslant 3, t)$. Correspondingly, the other two probability functions decrease over time. For $t/t_e \gtrsim 2$ the functions remain essentially stationary. Figure 4 is in very good qualitative agreement with Fig. 6 of WM. The quantitative differences are primarily due to a different number of particles in the simulations (WM: $n_p^r = 131072$, present work: $n_p^r = 147456$).

Our implementation of two-way coupling was validated in a previous publication by Bosse *et al.*[22] concerning the settling and break-up of suspension drops. The same two-way coupling algorithm was used for the present study.

IV. RESULTS

A. Settling velocity enhancement by collective particle drag

In order to study the effect of two-way coupling on the mean particle settling velocity, a set of simulations with varying particle volume fraction and otherwise fixed parameters was performed. The Stokes number St_η and the dimensionless terminal velocity U_p/u_η were set to unity, for which a strong interaction between dispersed phase and carrier fluid is to be expected. We chose a density ratio of $\varrho_p/\varrho = 5000$ for all simulations reported in this section, which was motivated by two reasons. First, there is a number of experimental investigations of solid particles in air turbulence, where ϱ_p/ϱ assumes typical values between 2500 (glass particles in air) and 9400 (lead particles in air); see, e.g., Schreck and Kleis[28] and Kulick *et al.*[29] So $\varrho_p/\varrho = 5000$ was taken as an intermediate density ratio, representative of these experimental conditions. The second reason is related to the computation of particle statistics. For a given particle volume fraction Φ_v and Stokes number St_η, an increased particle-fluid density ratio leads to a smaller particle diameter and therefore to a larger number of particles. In the case of very small particle loadings, this may be important to obtain reliable particle statistics. For example, for $\Phi_v = 1.5 \times 10^{-6}$ and a smaller particle-fluid density ratio $\varrho_p/\varrho = 1000$, we would obtain fewer than 3000 particles in the flow, which we considered insufficient for reliable statistics.

The range of particle volume fractions relevant for our investigation is $10^{-7} \lesssim \Phi_v \lesssim 10^{-4}$. The suspension at the lower bound of $\Phi_v \approx 10^{-7}$ is usually considered to be dilute enough to simulate the particle-fluid interaction in a one-way coupled approach (see, e.g., Elghobashi[25]). From $\Phi_v \approx 10^{-6}$ on, two-way coupling effects may become important. As known from the one-way coupled simulations presented above, the local volume fraction may increase during the simulation by about an order of magnitude compared to the mean volume fraction due to particle accumulation. Thus, the upper bound of $\Phi_v \approx 10^{-4}$ was chosen such that the expected maximum local volume fraction would not exceed $\Phi_v \approx 10^{-3}$. This value is usually considered the limit where particle-particle collisions (four-way coupling) become important, which are not included in our numerical model. The grid resolution was chosen as small as possible to save on computational time. For the range of volume fractions investigated and a sufficiently large number of particles (of order 10^5), an initial microscale Reynolds number of $\mathrm{Re}_\lambda \approx 40$ is necessary for a consistent set of parameters. Accordingly, the grid resolution was set to $N = 64$. The number of computational particles was $n_p^c = 100\,096$ in all simulations. To account for the increasing number of real particles with growing volume fraction, the ratio M of real to computational particles was adjusted accordingly.

A simulation for a specific particle volume fraction consists of three parts. First, the forcing parameters are chosen to yield a desired microscale Reynolds number Re_λ. The simulation is run without particles to yield the quasistationary turbulence characteristics, such as the eddy turnover time and the Kolmogorov scales, required to form the desired par-

ticle parameters, i.e., the Stokes number and the dimensionless terminal velocity. Second, the particles are released into the fluid starting from a uniformly random distribution and the simulation is run with one-way coupling only. This yields particle statistics for comparison with the two-way coupled case. Third, two-way coupling is included in the simulation starting from an instantaneous velocity and particle field of the foregoing one-way coupled run. This has the advantage that particle and (changing) fluid statistics converge more quickly than in a simulation started from a zero velocity field and random particle positions. To ensure that the particle initial conditions in the two-way coupling regime, i.e., the switching from one-way to two-way coupling, do not affect the long-term statistics, we also started a two-way coupled simulation from an instantaneous velocity field with a uniformly random particle distribution. Here, the particle velocity was set to the Stokes settling velocity. The differences in the computed settling velocities were found to be negligible compared to those obtained in the three-step procedure outlined above (e.g., $\Delta V_3/U_p=0.577$, $\Delta V_3/u'=0.183$ compared to run No. 2 in Table II; see below).

It should be noted that fluid turbulence quantities can change once the two-way coupling is active. Thus, the turbulence statistics characterized by Re_λ, η, t_e, etc. are only known *a posteriori*. (In particular, this can involve a tedious trial-and-error process to match certain experimental conditions.) In all simulations, it was ensured that the flow had reached a quasistationary state before computing the turbulence statistics both for one-way and two-way coupling. Note that in the two-way coupling regime, the flow is still homogeneous but no longer isotropic.

Figure 5 shows the time evolution of the mean particle velocities for two different particle volume fractions, $\Phi_v=1.5\times10^{-5}$ and $\Phi_v=1.5\times10^{-4}$ (initial $\mathrm{Re}_\lambda\approx42$, see also Table II, runs No. 2 and No. 7). At $t/t_{e,0}\approx50$ the phase coupling was switched from one-way to two-way coupling. Here, $t_{e,0}$ denotes the eddy turnover time in the one-way coupling regime. This time scale was chosen for nondimensionalization since the turbulence characteristics may change in the two-way coupling regime. For one-way coupling we observe an already increased mean particle settling velocity compared to the Stokes settling velocity. This is due to the mechanism of preferential sweeping as explained in the Introduction. Once the particles are allowed to exert a feedback force onto the fluid, a further, almost immediate enhancement of the mean settling velocity is found (at $t/t_e\approx50$). This enhancement is more pronounced in the case of the larger particle volume fraction, where the settling velocity is increased by a factor of about 2.3 compared to the Stokes velocity. In both cases, the mean particle velocities in directions x_1 and x_2 fluctuate around zero, which is in accordance with the isotropic conditions and a vanishing mean fluid velocity in planes perpendicular to the direction of gravity.

The local particle volume fractions Φ_v^l/Φ_v of the same simulations as in Fig. 5 are visualized in Fig. 6. The particle volume fraction is shown in a slice cut through the computational cube at $x_2=\pi$ at two different times, $t/t_e=25$ in the one-way coupling regime and $t/t_e=100$ in the two-way coupling regime. In the case of $\Phi_v=1.5\times10^{-5}$ there are no discernible differences in the overall qualitative structure of the inhomogeneous particle distribution. In both cases, the particles accumulate in certain regions where the local particle volume fraction can be up to about four times higher than the average volume fraction. The size of the typical particle-free areas is very similar in both cases. Thus, the visible structure of inhomogeneities in the particle distribution does not allow to infer whether one-way or two-way coupling is present. In the case of $\Phi_v=1.5\times10^{-4}$ the typical size of the particle-free regions appears somewhat smaller than in the previous case. This is due to a reduced microscale Reynolds number as a consequence of the particle-fluid interaction, which involves a smaller eddy length scale. Thus, the overall volume of the regions of high particle concentration (low vorticity) increases and the maximum particle volume fraction reduces to about 2.5 times the average. The turbulence modulation by the particles will be discussed further below.

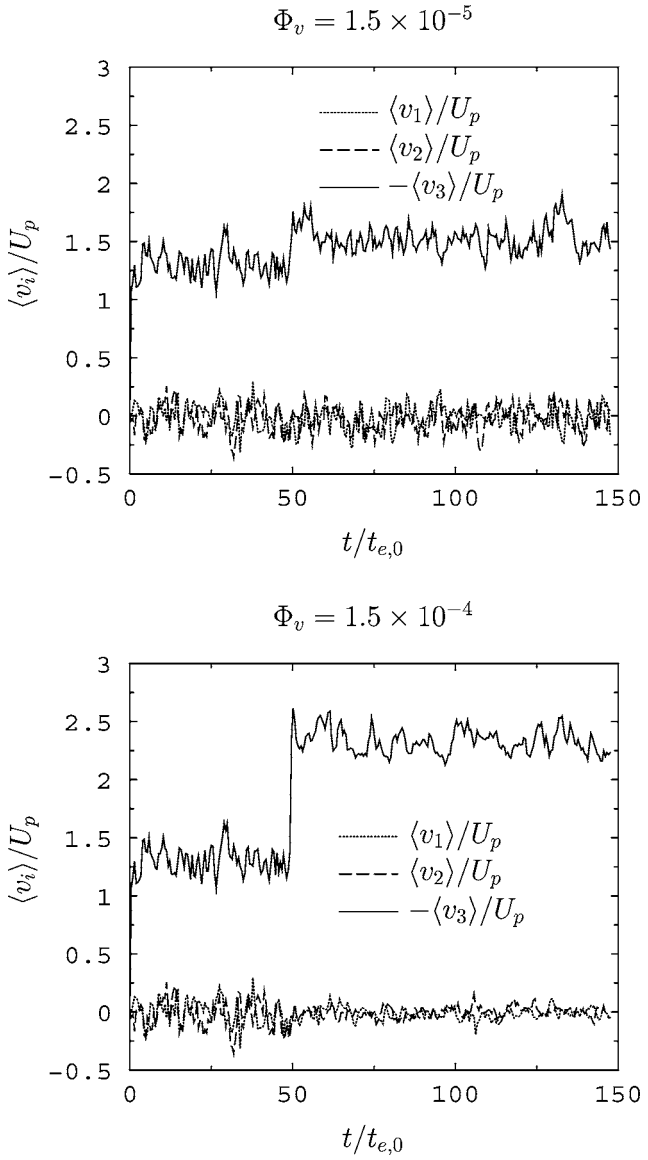

FIG. 5. Time evolution of mean particle velocities normalized by the terminal settling velocity U_p. At $t/t_{e,0}\approx50$ the phase coupling was switched from one-way to two-way coupling ($t_{e,0}$ denotes the eddy turnover time in the one-way coupling regime).

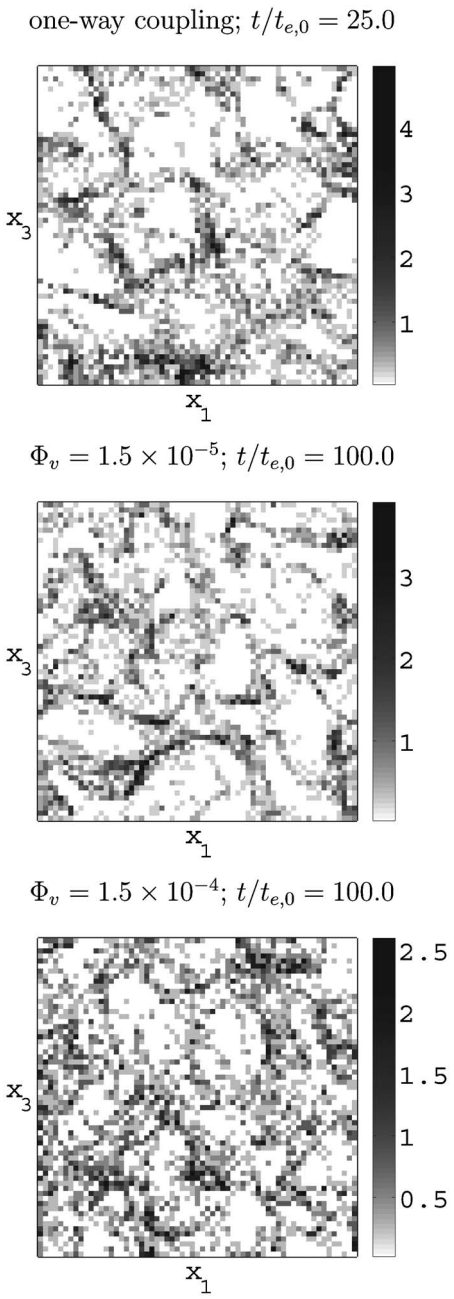

FIG. 6. Normalized particle volume fraction Φ_v^l/Φ_v in slices of thickness $3\Delta x_2$ cut through the center of the computational box (at $x_2=\pi$). Top: one-way coupling; middle and bottom: two-way coupling. Same simulations as shown in Fig. 5.

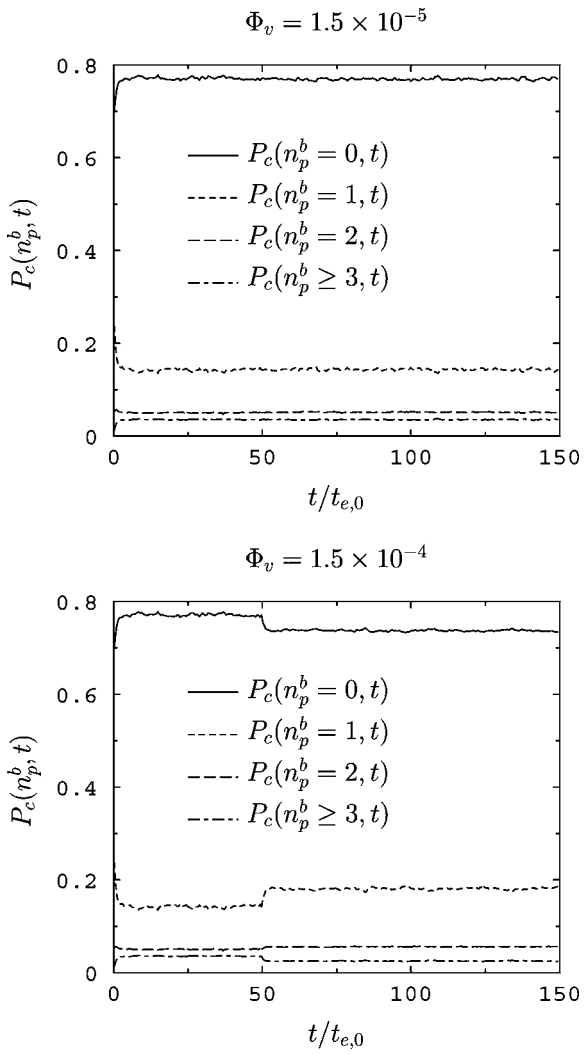

FIG. 7. Time evolution of the probability functions $P_c(n_p^b,t)$ for different particle volume fractions Φ_v. At $t/t_{e,0}\approx 50$ the phase coupling was switched from one-way to two-way coupling. Initial $\mathrm{Re}_\lambda=42$, $N=64$. Same simulations as shown in Fig. 5.

The time evolution of the probability functions $P_c(n_p^b,t)$ introduced in the previous section corroborates the qualitative observations of the particle dispersion (Fig. 7). Again, in the case of $\Phi_v=1.5\times10^{-5}$ there are no discernible differences between the one-way and the two-way coupling regime. In the case of $\Phi_v=1.5\times10^{-4}$ the onset of the two-way coupling regime is characterized by a small shift of all four probability functions displayed. According to the changing turbulence properties involving smaller eddy length scales, the probability of finding particle-free regions decreases slightly while that of finding one particle per cell increases. The occurrence of higher particle volume fractions changes only slightly.

Figure 8 shows the enhancement of the particle settling velocity as a function of the particle volume fraction in the case of two-way coupling. The range of particle volume fractions covered is $1.5\times10^{-6}\leqslant\Phi_v\leqslant1.5\times10^{-4}$ (see also Table II, runs No. 1 to No. 7). As before, the settling velocity difference ΔV_3 is normalized by either the Stokes settling velocity or the fluid rms velocity. If the particle volume fraction is very small, i.e., $\Phi_v\leqslant1.5\times10^{-6}$, the additional increase in the particle settling velocity is negligible compared to the one-way coupled regime. Thus, $\Phi_v\approx10^{-6}$ can be considered the limit where two-way coupling effects come into play and start affecting the fluid-particle interaction. This confirms common observations found in the literature, see, e.g., Elghobashi.[25] The enhancement of the settling velocity is nonzero for $\Phi_v\leqslant1.5\times10^{-6}$ due to the preferential sweeping effect, as explained in the Introduction.

As long as the overall turbulence properties are not significantly influenced by the feedback forces of the particles, the enhancement of the particle settling velocity increases with a roughly constant slope as a function of the particle

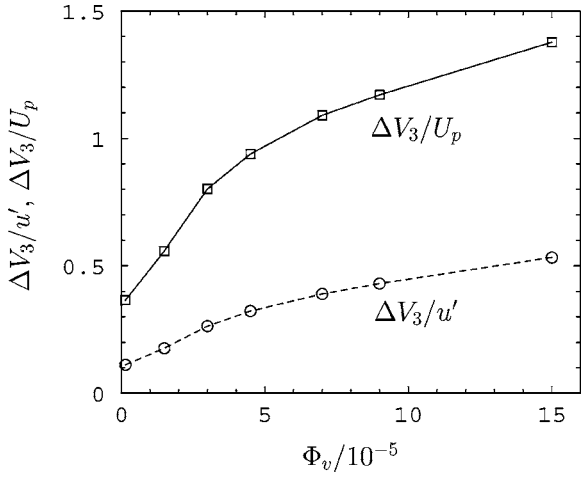

FIG. 8. Particle settling velocity enhancement as a function of the particle volume fraction (two-way coupling). Simulations were started from a fully turbulent flow field with one-way coupled particles. Initial parameters: $\mathrm{Re}_\lambda=42$, $\mathrm{St}_\eta=1.0$, $U_p/u_\eta=1.0$. $N=64$ in all cases.

volume fraction. This is observed for $1.5\times10^{-6}\leqslant\Phi_v\leqslant3\times10^{-5}$ in Fig. 8. In this range the particle and turbulence properties remain roughly constant for fixed forcing parameters (see also Table II and discussion of turbulence modification below). If the particle volume fraction is further increased, the slope of the curve decreases. The strongest velocity enhancement is found for the largest particle volume fraction in the range covered, $\Phi_v=1.5\times10^{-4}$. Here, the increase is almost 1.5 times the Stokes settling velocity.

For all simulations the particle velocity enhancement and some turbulence properties are summarized in Table II. The overall observation is that the introduction of small particles into the turbulent carrier fluid has a dissipative effect on the turbulence for particle volume fractions $\Phi_v\gtrsim3\times10^{-5}$. This involves a change of essentially all relevant turbulent quantities, such as the turbulent kinetic energy and dissipation rate, the Kolmogorov scales, the eddy length and time scale, and other integral scales. As a result, the microscale Reynolds number drops below its value in the one-way coupled case, reflecting a decrease in the overall turbulence "level." It is worth emphasizing that for the current density ratio of $\varrho_p/\varrho=5000$, turbulence modification is seen to occur for particle volume fractions as low as $\Phi_v\approx5\times10^{-5}$. On the other hand, Aliseda *et al.*[18] report that for their experimental conditions of $\varrho_p/\varrho=1000$, turbulence modification was not observed even for volume fractions of up to $\Phi_v\approx7\times10^{-5}$.

For a better illustration of the turbulence modulation with increasing particle volume fraction, some characteristic turbulent quantities are displayed separately in Fig. 9. The microscale Reynolds number Re_λ decreases due to a decrease of both the rms velocity u' and the Taylor microscale λ [Figs. 9(a)–9(c)]. It is interesting to note that the Kolmogorov scales hardly change with increasing particle volume fraction, whereas the eddy turnover time t_e and length scale l_e decrease considerably (by up to 58%, Table II). The former observation indicates that the particles interact primarily with turbulent structures larger than the smallest ones. Indeed, the visualization in Fig. 5 suggests a typical length scale of the particle inhomogeneities larger than the Kolmogorov length. As shown by Wang and Maxey,[15] Yang and Lei,[17] and others, this length scale is of the order of 10η, which is consistent with Fig. 5. In fact, Yang and Lei demonstrated that the preferential accumulation can accurately be predicted in a large-eddy simulation (LES) with the Kolmogorov scales not

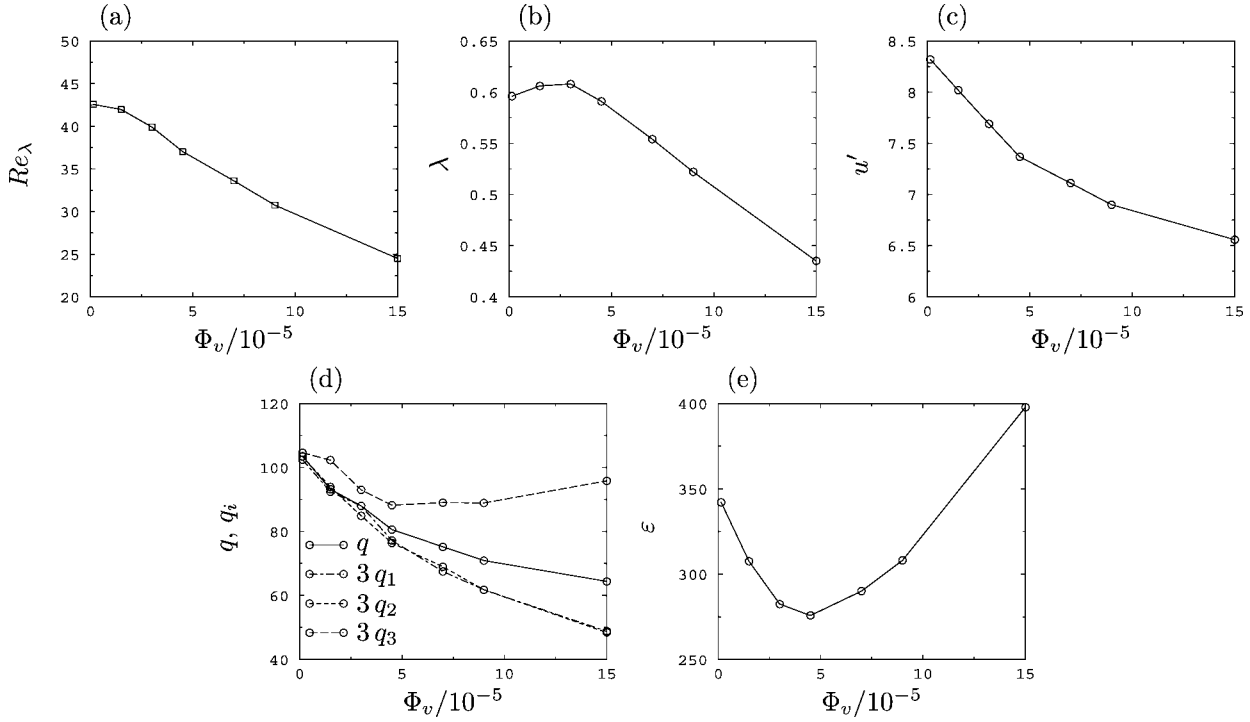

FIG. 9. Different mean turbulence properties as a function of the particle volume fraction (same set of simulations as in Fig. 8). (a) microscale Reynolds number Re_λ; (b) Taylor microscale λ; (c) rms velocity u'; (d) mean turbulent kinetic energy q and energies q_i averaged in directions i; (e) dissipation rate ε.

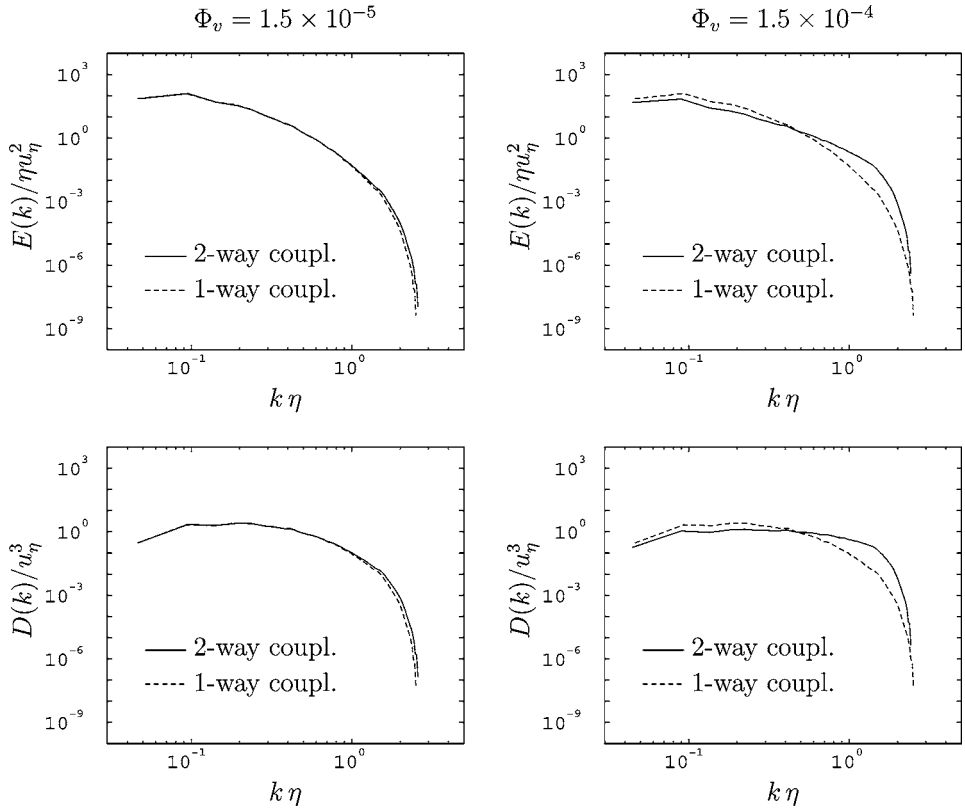

FIG. 10. Three-dimensional energy spectra (top) and dissipation spectra (bottom) for $\Phi_v = 1.5 \times 10^{-5}$ (left) and $\Phi_v = 1.5 \times 10^{-5}$ (right) in the case of one-way and two-way coupling.

resolved by the computational grid. The decrease of the eddy time and length scales, on the other hand, is primarily due to the damped velocity fluctuations u' (cf. their definitions in Sec. II D). Note that the damped velocity fluctuations are also observed in Fig. 5 for $\Phi_v = 1.5 \times 10^{-4}$ and $t/t_{e,0} > 50$.

The presence of gravity introduces an anisotropy that alters the initially isotropic fluid velocity field by particle drag forces. This becomes obvious when comparing the turbulent kinetic energies q_i associated with the three spatial directions [Fig. 9(d)]. While the energies in the directions perpendicular to gravity are reduced with increasing Φ_v, the energy in the direction of particle settling remains roughly constant for $\Phi_v \gtrsim 3 \times 10^{-5}$. Thus, despite an overall reduction in turbulent kinetic energy, the energy, and therefore the velocity fluctuations, in the direction of gravity are increased compared to the other directions. It should be noted that Ferrante and Elghobashi[30] also found an augmentation of the velocity fluctuations in direction of gravity. In the case of decaying homogeneous turbulence and for $\mathrm{St}_\eta = 0.25$ and $U_p^* = 0.25$, this leads to a reduction in the decay rate of turbulence. In their recent experiments, Yang and Shy[20] found turbulence augmentation in the gravitational direction for most frequencies, whereas in the transverse directions, augmentation occurred only at higher frequencies beyond the Taylor microscale for values of St_η varying from 0.36 to 1.9.

The dissipative effect of the particles is most evident in the mean turbulent kinetic energy q, which is significantly reduced with growing particle volume fraction. The dissipation rate ε, however, decreases for volume fractions $\Phi_v \lesssim 5 \times 10^{-5}$ corresponding to the beginning decrease in the overall turbulence level, and then increases again for higher volume fractions [Fig. 9(e)] once the particles start developing their dissipative effect. For $\Phi_v = 1.5 \times 10^{-4}$ the dissipation rate is even larger than in the one-way coupled case. This is only possible because the particles interact primarily with the small-scale fluid structures (although not with the smallest ones as discussed above). That means the particles' effect is not uniform but selective with respect to the range of represented wave numbers. This can be confirmed by analyzing the energy and dissipation spectra, which are plotted in Fig. 10 for particle volume fractions $\Phi_v = 1.5 \times 10^{-5}$ and $\Phi_v = 1.5 \times 10^{-4}$. In the first case, the influence of the particles on the spectral distribution of turbulent kinetic energy and dissipation is negligible. Correspondingly, the turbulence properties are essentially not affected by the presence of the particles (Table II, run No. 2). In the second case, with the particle volume fraction larger by one order of magnitude, we observe a significant spectral redistribution of kinetic energy with respect to the shape of the spectra. The energy and dissipation associated with the small scales (high wave numbers) increase, while those associated with the large scales decrease. This phenomenon is sometimes referred to as "pivoting" and has been reported in the literature by different authors (e.g., Squires and Eaton,[8] Elghobashi and Truesdell,[9] and Sundaram and Collins[31]). Since turbulence modification is not the focus of this study, we refrain from a more detailed analysis at this point.

Figure 11 shows the enhancement of the particle settling

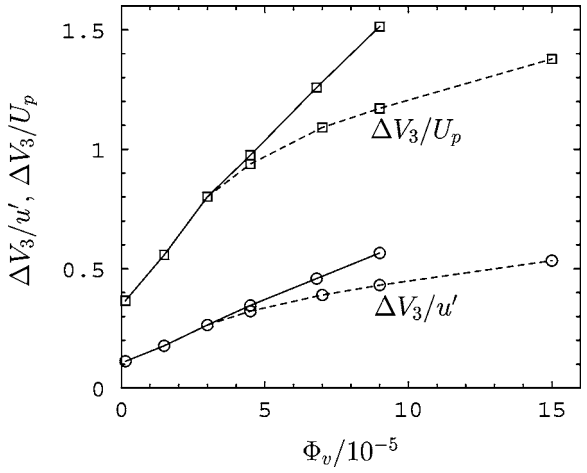

FIG. 11. Particle settling velocity enhancement as a function of the particle volume fraction. Solid lines: Reynolds number remains fixed at $\mathrm{Re}_\lambda \approx 42$ (forcing parameters adjusted accordingly). Dashed lines: Reynolds number decreases due to turbulence modulation by the particles, same as shown in Fig. 8 (fixed forcing parameters). $\mathrm{St}_\eta \approx 1.0$, $U_p/u_\eta \approx 1.0$ in all cases.

velocity over the particle volume fraction if the microscale Reynolds number is fixed at $\mathrm{Re}_\lambda \approx 42$. For comparison, the dashed lines indicate the same relation in the case where the microscale Reynolds number reduces with increasing particle volume fraction due to turbulence modulation by the particles (as already discussed, cf. Fig. 8). In the former case, the forcing parameters were adjusted for each run separately such that the resulting turbulence level in the two-way coupling regime was $\mathrm{Re}_\lambda \approx 42$, whereas in the latter case all simulations were performed with fixed forcing parameters (Table III contains the grid resolutions and forcing Reynolds numbers for the additional simulations in Fig. 11). The increase in the particle settling velocity enhancement is found to have a nearly constant slope over the range investigated if the (resulting) microscale Reynolds number is kept constant. This result is in good agreement with the findings by Aliseda *et al.*[18] (see their Fig. 16). Also, it shows that the particle velocity enhancement does not only depend on the particle loading, but also on the Reynolds number of the turbulent carrier flow.

In order to understand the physical mechanism responsible for the particle settling velocity enhancement, the collective effect of the particles in regions of increased particle volume fraction needs to be analyzed. To this end, the mean

TABLE III. Data of simulations with fixed $\mathrm{Re}_\lambda \approx 42$ in Fig. 11 (the data corresponding to the dashed lines are given in Table II). Forcing parameters: $\varepsilon^* = 16.997$, $T_L = 0.038$, $K_F = 2\sqrt{2}$.

Φ_v	4.5×10^{-5}	6.8×10^{-5}	9.0×10^{-5}
Re^*	11.96	12.99	16.70
N	72	72	96
Re_λ	42.5	41.5	41.9
$k_{\max}\eta$	1.30	1.29	1.36
$\Delta V_3/U_p$	0.975	1.258	1.514
$\Delta V_3/u'$	0.346	0.459	0.566

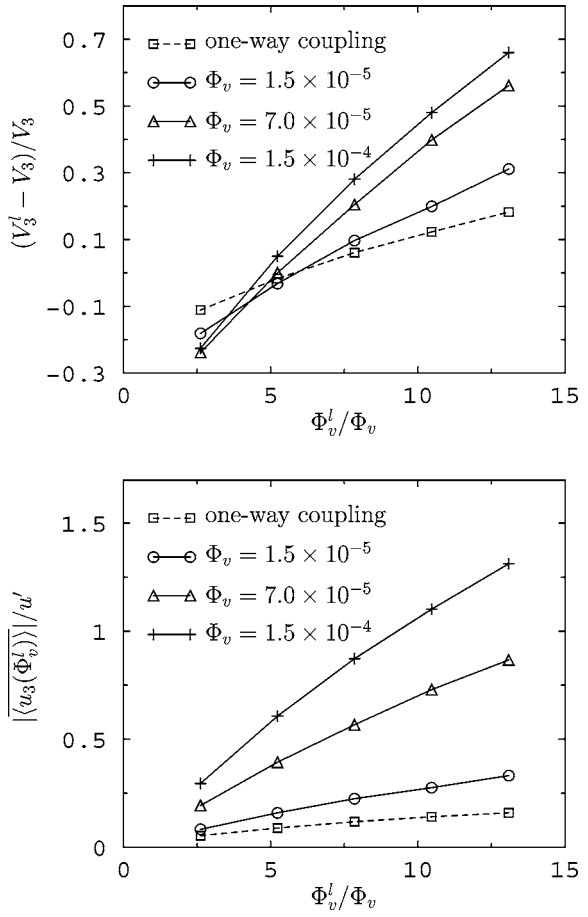

FIG. 12. Top: Mean particle settling velocity averaged over regions of certain local particle volume fraction Φ_v^l for different overall particle loadings Φ_v. Bottom: Magnitude of the mean fluid velocity $\overline{\langle u_3\rangle}$ in these regions. The dashed lines show the one-way coupled case for comparison. $\mathrm{St}_\eta \approx 1.0$, $U_p/u_\eta \approx 1.0$ in all cases. Re_λ according to Table II.

particle settling velocity conditioned to the regions of increased local particle concentration will be compared for one-way and two-way coupling and different overall particle volume fractions. The same is done for the mean fluid velocity in these regions.

In the following, the mean particle settling velocity averaged over the whole computational domain and over time is denoted by

$$V_3 := \overline{\langle v_3\rangle}, \tag{22}$$

where the angle brackets indicate an average over all particles and the overbar denotes a time average. Similarly, the mean particle settling velocity averaged over regions of a specific local particle volume fraction is denoted by

$$V_3^l(\Phi_v^l) := \overline{\langle v_3(\Phi_v^l)\rangle}. \tag{23}$$

Figure 12 shows the normalized difference of the conditioned mean particle settling velocity $V_3^l(\Phi_v^l)$ to the overall mean settling velocity V_3 for the simulations summarized in Table II. Furthermore, the corresponding mean fluid velocity magnitude in the x_3 direction in these regions of specific Φ_v^l is shown in the bottom graph of Fig. 12 (note that $\overline{\langle u_3\rangle}$, i.e., u_3 averaged over the entire domain, is zero by definition). As

mentioned before, the number of boxes in which the local quantities were computed is equal to the number of grid cells ($N_b=N^3$). The normalized local particle concentration is only shown for a range up to $\Phi_v^l/\Phi_v \approx 13$. Although areas of even larger local particle concentration are found, their number of occurrences is rather small, resulting in poor statistics. For this reason, these very high local particle concentrations are excluded from Fig. 12.

We observe a monotonic increase in the conditioned settling velocity with increasing local particle volume fraction for both one-way and two-way coupling. However, this effect is much stronger in the case of two-way coupling and is enhanced with increasing overall particle volume fraction Φ_v. Thus, in the case of two-way coupling we observe a collective effect of the particles in regions of high particle concentration, resulting in an enhanced mean settling velocity in these regions. The accumulated particles—pulled downwards by gravity—exert a larger drag force on the surrounding fluid, which is more accelerated in the negative x_3 direction than in the one-way coupled case. This is seen in the bottom graph. Here, the magnitude of the mean fluid velocity $|\overline{\langle u_3(\Phi_v^l)\rangle}|$ averaged over regions of a specific particle volume fraction Φ_v^l is found to exhibit a similar monotonic increase due to the particle-fluid interaction (the fluid velocity u_3 in all regions where particles are found is negative on average). The particle settling velocity in regions of high particle concentration increases, because the particles settle relatively to downward-accelerated fluid. The coupling between particles and fluid together with gravity results in an increase of both the particle settling velocity and the fluid downward velocity in regions of high particle concentration. Note that the curves for the particle velocity enhancement in the upper graph cross each other at $\Phi_v^l/\Phi_v \approx 4$. This is due to the normalization by the overall mean settling velocity V_3, which increases with increasing particle volume fraction Φ_v. It indicates that the effect of the accumulated particles becomes more important with both growing local and overall particle concentration.

If the microscale Reynolds number Re_λ is kept constant as in Fig. 11 (solid lines), the qualitative behavior of the conditioned particle and fluid velocities remains the same as that in Fig. 12. However, the slopes of the curves for particle volume fractions $\Phi_v \gtrsim 3.0\times10^{-5}$ are a little steeper than in Fig. 12.

The mechanism responsible for the particle velocity enhancement in two-way coupled simulations can now be explained as the interplay of three contributing effects. The first one is the well-known inertial bias by which the particles accumulate in regions of high-strain rate and low vorticity. If gravity is present, the second effect, usually known as preferential sweeping, causes the particles to travel primarily toward regions of downward fluid motion on their way through the turbulent carrier flow. This can also be observed in merely one-way coupled simulations. Finally, the third effect—only present in the case of two-way coupling—is a local modification of the fluid velocity structure by the particles in regions of increased particle volume fraction. The collective effect of the accumulated particles is a downward drag force on the carrier fluid. As a result, the latter is additionally accelerated in the direction of gravity compared to the one-way coupled case, which in turn causes the particle settling velocity to be enhanced in these regions of increased downward fluid motion. In principle, this explanation is similar to the phenomenological model hypothesized by Aliseda *et al.*[18] Their model is based on the assumption of individual particle clusters acting as large pseudoparticles and settling at their own velocity V_{cl}, which adds to the mean settling velocity of an isolated particle in turbulence. According to Fig. 5, such individual clusters cannot be clearly identified in our simulations. Rather, the particles appear to accumulate in coherent, web-like regions of low vorticity.

TABLE IV. Stokes numbers and corresponding dimensionless Stokes settling velocities investigated by Aliseda *et al.* (Ref. 18) and used in our one-way coupled simulations presented in Fig. 14.

St_η	0.18	1.0	1.38	3.2
U_p/u_η	0.110	0.611	0.843	1.954

From the above considerations, it is clear that a certain degree of preferential particle accumulation is necessary for an additional settling velocity enhancement. For both one-way and two-way coupling, the preferential sweeping is most pronounced for particle Stokes numbers around unity. This has been shown by a number of researchers, including the experimental studies by Aliseda *et al.*[18] and Yang and Shy,[20] and it was confirmed in our simulations (not shown). Thus, a Stokes number around unity is a precondition for a significant additional enhancement of the particle settling velocity to be observed. In order to study the influence of the second parameter in the particle equation of motion, the dimensionless Stokes velocity, we chose a particle volume fraction of $\Phi_v=3.0\times10^{-5}$ and four different values of U_p^* ($\mathrm{St}_\eta=1$, $\mathrm{Re}_\lambda \approx 40$). The results are shown in Fig. 13. Here, we observe a different behavior of the settling velocity enhancement, depending on whether the Stokes velocity U_p or the rms velocity u' is used for nondimensionalization. In the first case, the settling velocity enhancement decreases with increasing U_p/u_η, while in the second case it increases.

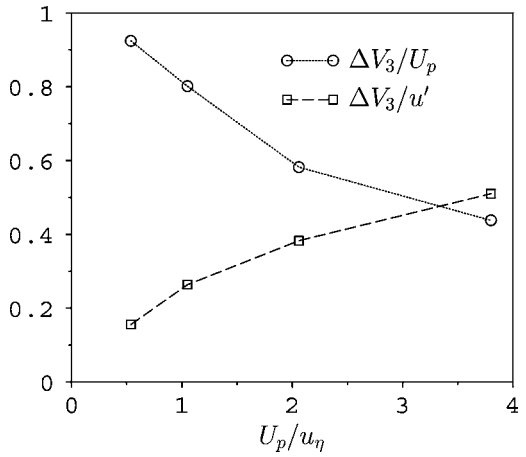

FIG. 13. Settling velocity enhancement as a function of the dimensionless Stokes settling velocity. $\Phi_v=3.0\times10^{-5}$, $\mathrm{St}_\eta=1$, $\mathrm{Re}_\lambda \approx 40$. Same forcing parameters as in Table II.

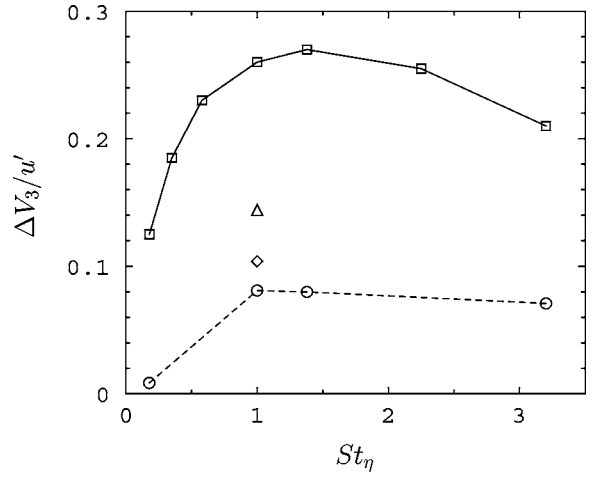

FIG. 14. Increase in the mean particle settling velocity as a function of the Stokes number. Comparison of simulations with the experiment of Aliseda *et al.* for $\mathrm{Re}_\lambda=75$; one-way coupled simulations (dashed lines); experiment, $\Phi_v=1.5\times10^{-5}$ (solid lines); two-way coupled simulations: $\diamond$ $\Phi_v=1.5\times10^{-5}$, $\triangle$ $\Phi_v=7.0\times10^{-5}$.

The influence of the particle-fluid density ratio was examined in two simulations with (a) $\varrho_p/\varrho=3500$ ($M=3.91$) and (b) $\varrho_p/\varrho=2000$ ($M=1.69$) and otherwise the same parameters as in run No. 3 of Table II. It was found that the mean particle settling velocity slightly decreases with decreasing density ratio: (a) $\Delta V_3/U_p=0.668$, $\Delta V_3/u'=0.217$, $\mathrm{Re}_\lambda=40.8$; (b) $\Delta V_3/U_p=0.578$, $\Delta V_3/u'=0.181$, $\mathrm{Re}_\lambda=42.1$. However, this effect is much less significant than the influence of the other parameters discussed above.

B. Comparison with experimental results

In the previous section, it was shown that the mean particle settling velocity in homogeneous turbulence can be considerably increased due to a collective effect of the particles in regions of high particle concentration. In the following, a quantitative comparison of these findings with the experimental results by Aliseda *et al.*[18] and Yang and Shy[20] will be performed.

Aliseda *et al.*[18] (hereafter referred to as AL) conducted experiments of heavy particles settling in homogeneous decaying turbulence. Their experimental facility was a wind tunnel, in which roughly spherical water droplets of different size were seeded into a grid-generated turbulent airstream. They provide turbulence and particle statistics at two downstream locations of the wind tunnel, corresponding to microscale Reynolds numbers of $\mathrm{Re}_\lambda=75$ and 48, respectively. We chose the first one for a direct comparison, by matching the microscale Reynolds number in our simulations to that in the experiment.

In a first set of simulations, the mean particle settling velocity was investigated for $\mathrm{Re}_\lambda=75$ ($N=128$) in a one-way coupled approach. Several Stokes numbers and corresponding dimensionless terminal settling velocities [see Eq. (10)] were studied according to Table IV. The density ratio was set to $\varrho_p/\varrho=1000$ in all simulations. Figure 14 and Table V show the increase in the mean particle settling velocity as a function of the Stokes number for both our simulations and the experiment (with the approximate values for $\Phi_v=1.5\times10^{-5}$ taken from Fig. 14 of AL). It is obvious that one-way coupling between the fluid and dispersed phase is not sufficient to capture the underlying physics of the enhanced particle settling. The simulation results under-predict the experimental findings by a factor of about 3 at $\mathrm{St}_\eta\geqslant1$ and more than an order of magnitude for $\mathrm{St}_\eta=0.18$.

For the two-way coupled case, two simulations with $\Phi_v=1.5\times10^{-5}$ and $\Phi_v=7.0\times10^{-5}$ were performed, which are also shown in Fig. 14 ($\mathrm{Re}_\lambda=75$, $\mathrm{St}_\eta=1$, $U_p/u_\eta=0.6$). In the first case, we observe an increase in the particle settling velocity of roughly 30% compared to the one-way coupled case. However, the predicted velocity enhancement of $\Delta V_3/u'\approx0.1$ is still considerably smaller than the experimental result of $\Delta V_3/u'\approx0.26$. If the particle volume fraction is augmented to $\Phi_v=7.0\times10^{-5}$, the settling velocity enhancement increases further, as expected, but the discrepancy between experimental and numerical results is still observed [AL: $\Delta V_3/u'\approx0.46$ (not shown in Fig. 14), present work: $\Delta V_3/u'\approx0.14$].

As will be discussed below, the mean particle settling velocities measured by Yang and Shy[20] are much smaller than the results of AL. Yang and Shy list several potential reasons for this discrepancy, such as the fact that the turbulence intensity in AL is much smaller than the mean flow, and that it rapidly decreases in the streamwise direction. This might make it difficult to determine the effective settling velocity accurately. Nevertheless, the discrepancies between AL and our simulations call for a discussion of possible reasons, which is done in the following.

In the experiment by AL, the turbulent air stream in the wind tunnel was seeded with particles generated by an array of atomizers. The particle size was not uniform, but spread over a range of diameters (Fig. 3 of AL displays the probability density function of the droplets' diameter). Thus, particles with different Stokes numbers ranging from $\mathrm{St}_\eta\approx0.01$ to 5.1 were present in the flow. In the simulations, on the other hand, all particles had the same Stokes number. This may be the most important difference between experiment and simulation. However, confining the particles to a single size with $\mathrm{St}_\eta=1$, for which the strongest particle-fluid interaction can be expected, should increase the effect of settling velocity enhancement rather than decrease it. This makes the particle size distribution unlikely to be the reason for the observed discrepancies.

In the simulations, linear interpolation was used to compute both the fluid velocity at the particle positions and the particle feedback forces at the grid points. The influence of interpolation has been a subject of controversy in the literature. Several authors use high-order interpolation to compute the fluid velocities, while considering low-order interpolation sufficient for the feedback forces (e.g., Ferrante and Elghobashi[13]). Others report no significant differences in the results whether high-order or low-order interpolation is used to compute the fluid velocities (e.g., Squires and Eaton[7]). For a general discussion on the influence of interpolation, the reader is referred to Balachandar and Maxey,[32] Yeung and Pope,[33] and Sundaram and Collins.[34] To assess the influence of fluid interpolation in our case, two simulations using spec-

TABLE V. Comparison of settling velocity enhancement computed in the present work (present) with Aliseda *et al.* (Ref. 18) (AL). Experimental values taken from Fig. 14 of AL for $\mathrm{Re}_\lambda=75$, $\Phi_v=1.5\times10^{-5}$. Simulations done with a grid resolution of $N=128$. Forcing parameters: $\varepsilon^*=16.997$, $T_L=0.038$, $K_F=2\sqrt{2}$, $\mathrm{Re}^*=24.49$.

		St_η	0.18	1.0	1.38	3.2
AL		$\Delta V_3/u'$	0.125	0.26	0.27	0.21
Present	(One-way)	$\Delta V_3/u'$	0.0086	0.081	0.080	0.073
		$\Delta V_3/U_p$	0.34	0.56	0.37	0.16
	(Two-way)	$\Delta V_3/u'$		0.104		
		$\Delta V_3/U_p$		0.732		

tral summation and fourth-order Lagrangian polynomials were performed and compared with corresponding simulations presented in the previous sections for one-way and two-way coupling, respectively. (Due to computational limitations, we resort here to two representative simulations using smaller grid resolutions than required for a direct comparison with the simulations in Table V, which were done on a 128^3 grid.) As shown in Table VI, higher-order interpolation does have a certain influence on the results. In the case of two-way coupling, the particle velocity enhancement is roughly 5% smaller if fourth-order accurate polynomials are used instead of linear interpolation. In the previous section on the effects of two-way coupling on the particle settling, this difference is acceptable, since we were primarily interested in demonstrating the principal mechanism of additional settling velocity increase compared to the one-way coupled case. When comparing with experimental results, such a difference can be important. However, Table VI suggests a tendency of higher-order interpolation to decrease the mean particle settling velocity compared to linear interpolation. Moreover, even when assuming a 20% change in velocity (as obtained in the one-way coupled case, Table VI), this difference is much smaller than that found in Fig. 14. Thus, linear interpolation cannot be responsible for the observed discrepancies between simulation and experiment.

As for the experimental conditions, there is one somewhat speculative remark to be made about the measurement of the mean particle settling velocity. It would be conceivable that the settling particles in the experiment induce a non-negligible mean downward fluid velocity within the measurement region of the wind tunnel cross section. This mean downward fluid motion would be balanced by an upward motion near the tunnel walls outside the measurement region. Clearly, if measured with respect to the fixed laboratory system, the particle settling velocity would then be overestimated compared to the simulation. However, the paper by AL does not provide any information regarding this issue.

TABLE VI. Particle velocity enhancement computed with different fluid interpolation methods (LIN: linear, CUB: third-order Lagrangian polynomials, SPE: spectral summation). One-way coupling: $N=32$, $\mathrm{Re}_\lambda=21$, $\mathrm{St}_\eta=1$, $U_p/u_\eta=1$. Two-way coupling: run No. 2 from Table II.

		LIN	SPE
(One-way)	$\Delta V_3/u_\eta$	0.155	0.125
		LIN	CUB
(Two-way)	$\Delta V_3/u'$	0.177	0.168

At the same time, one needs to keep in mind that the present simulations involve some general approximations and assumptions. For example, a direct numerical simulation at $\mathrm{Re}_\lambda \gtrsim 75$ typically involves only three to four large eddies, which is certainly less than in a corresponding experiment. Also, even though the details of the forcing procedure were shown by Eswaran and Pope to have no effect on the small-scale statistics, the forcing acting on the large scales as an energy input is a numerical artifact, which is not present in real turbulence. These are general limitations of the employed numerical simulation approach.

As mentioned in the Introduction, Yang and Shy[20] (hereafter referred to as YS) conducted experiments of particles settling in stationary, near-isotropic turbulence using a cruciform apparatus consisting of a vertical and a horizontal vessel. Two counter-rotating fans at the ends of the horizontal vessel were used to generate the turbulence. Particles of a selected size were provided by a particle feeder and descended through the vertical vessel into the test region. As pointed out by YS, this setup may be more suitable for accurately measuring the mean particle settling velocity, since the particles are not influenced by a mean fluid flow and the turbulence is stationary, instead of decaying as in a wind tunnel. The enhancement of the particle settling velocity found by YS is generally much smaller than that determined by AL. YS compare their results with one-way coupled simulations by Yang and Lei.[17] However, a direct comparison is difficult since the parameters in the experiments and the simulations do not match exactly. For example, YS compare their results for $\mathrm{Re}_\lambda=73$ and $U_p/u_\eta=3.5$ with simulations by Yang and Lei at $\mathrm{Re}_\lambda=65$ and $U_p/u_\eta=3.0$. As we have seen in the previous section, both parameters have an influence on the mean particle settling velocity.

The overall particle volume fraction in all the experiments of YS was $\Phi_v\approx5\times10^{-5}$. For a direct comparison, we chose the measurements at $\mathrm{Re}_\lambda=73$ and $U_p/u_\eta=3.5$ ($\mathrm{St}_\eta=0.85$, $n_p^c=200\,192$, $M=6.035$, $\varrho_p/\varrho=1000$ in the simulations). The results are summarized in Table VII. For both one-way and two-way coupling, the predicted settling velocity enhancement is larger than in the experiment by YS. In the case of two-way coupling, we observe a significant additional increase of about 100% (from $\Delta V_3/U_p=0.18$ to $\Delta V_3/U_p=0.38$). The microscale Reynolds number decreases slightly with respect to the one-way coupled case, which is

TABLE VII. Comparison of settling velocity enhancement computed in the present work (present) with Yang and Shy (Ref. 20) (YS). Experimental values taken from Fig. 15 of YS for $\mathrm{Re}_\lambda = 73$; $\Phi_v = 5 \times 10^{-5}$. Simulations done with a grid resolution of $N = 128$. Forcing parameters: $\varepsilon^* = 16.997$, $T_L = 0.038$, $K_F = 2\sqrt{2}$, $\mathrm{Re}^* = 24.49$.

		Re_λ	St_η	U_p/u_η	$\Delta V_3/U_p$
YS		73	0.85 ± 0.2	3.5	0.13 ± 0.04
Present	(One-way)	74	0.85	3.5	0.18
	(Two-way)	71	0.85	3.5	0.38

due to a weak turbulence modification by the particles. The effect is very small, however, such that the resulting turbulence level at $\mathrm{Re}_\lambda = 71$ can still be compared with the experimental conditions at $\mathrm{Re}_\lambda = 73$. Thus, in contrast to the foregoing comparison with the experiment by AL, the experimental results by YS are overpredicted by our simulations.

YS did further experiments at $\mathrm{Re}_\lambda = 120$ and 202. These microscale Reynolds numbers require significantly larger numerical resolutions in a direct numerical simulation, which were beyond the computational limitations of the present study.

The above considerations suggest that additional research is required to clarify the discrepancies between different experiments on the one hand, and simulations and experiments on the other. At this point it is fair to say that establishing the correct mean particle settling velocity in a homogeneously turbulent carrier fluid requires additional experimental and computational work.

V. SUMMARY AND CONCLUSIONS

The settling of an initially random particle suspension in homogeneous turbulence was examined numerically, with the focus on the mean particle settling velocity. In the case of one-way coupling, the study by Wang and Maxey[15] was used for validation purposes. The increase of the mean settling rate of the particle suspension, compared to the terminal velocity of a single particle, was most pronounced for Stokes numbers around unity. Particles were shown to concentrate preferentially in regions of low vorticity. These findings are in very good agreement with the results by Wang and Maxey.

In the case of two-way coupling, the mean particle settling velocity was analyzed for different particle volume fractions Φ_v. We provide a number of quantities and correlations, which are difficult to determine in experiments, and which may thus contribute to clarifying the dynamics of particle settling in turbulence. The principal observation was an additional enhancement of the mean settling velocity, as compared to the one-way coupled case for volume fractions $\Phi_v \gtrsim 10^{-5}$. In regions of high concentration, the particles exert a collective effect on the carrier fluid, by which the fluid is accelerated due to particle drag. The enhanced downward fluid motion, in turn, leads to a larger particle settling velocity in these regions, thus increasing the overall mean settling velocity. In the range of particle volume fractions studied, $1.5 \times 10^{-6} \leqslant \Phi_v \leqslant 1.5 \times 10^{-4}$, the settling velocity enhancement monotonically grows with growing volume fraction. If the microscale Reynolds number Re_λ is kept constant, the increase has a roughly constant slope. These findings qualitatively agree with those by Aliseda *et al.*[18] If the forcing parameters are kept constant throughout the simulations for different particle volume fractions, the settling velocity enhancement grows less strongly, in particular for volume fractions $\Phi_v \gtrsim 3.0 \times 10^{-5}$. This is paralleled by a reduction of the turbulence intensity due to the particle-fluid interaction. The overall effect of the particles on the turbulence is dissipative, i.e., the mean turbulent kinetic energy is reduced. The effect, however, is selective with respect to the energy spectrum: at high wave numbers the energy (and dissipation rate) is increased, whereas at low wave numbers it is decreased. This is in accordance with results in the literature.

A careful quantitative comparison with experimental findings by Aliseda *et al.*[18] and Yang and Shy[20] was performed by matching the turbulence and particle parameters to those in the experiments. These two research groups provide quite different results for the mean particle settling velocity in homogeneous turbulence. In comparison with Aliseda *et al.*, our simulations underpredicted the experimental values ($\Delta V_3/u' = 0.10$ vs $\Delta V_3/u' = 0.26$ for $\mathrm{Re}_\lambda = 75$), whereas in comparison with Yang and Shy the computed mean particle settling velocity was considerably larger than the experimental results ($\Delta V_3/U_p = 0.38$ vs $\Delta V_3/U_p = 0.13$ for $\mathrm{Re}_\lambda \approx 73$). Some possible reasons for this discrepancy were discussed, in particular with respect to the investigation by Aliseda *et al.* Hence, establishing the correct mean particle settling velocity in a homogeneously turbulent carrier flow, and unraveling the underlying physical mechanisms, will require additional, close collaborations between experimentalists and computational modelers. In this respect it would be interesting, for example, to measure not only the mean particle settling velocity in regions of increased local particle volume fraction, but also the mean downward fluid motion in these areas, in order to allow a more detailed comparison with the simulation data.

ACKNOWLEDGMENT

The simulations were performed at the Swiss National Supercomputing Centre (CSCS) in Manno, Switzerland.

[1] K. D. Squires and J. K. Eaton, "Measurements of particle dispersion obtained from direct numerical simulations of isotropic turbulence," J. Fluid Mech. **226**, 1 (1991).
[2] S. Elghobashi and G. C. Truesdell, "Direct simulation of particle dispersion in a decaying isotropic turbulence," J. Fluid Mech. **242**, 655 (1992).
[3] J. K. Eaton and J. R. Fessler, "Preferential concentration of particles by turbulence," Int. J. Multiphase Flow **20**, 169 (1994).
[4] C. T. Crowe, T. R. Troutt, and J. N. Chung, "Numerical models for two-phase turbulent flows," Annu. Rev. Fluid Mech. **28**, 11 (1983).

[5]F. Wen, N. Kamaly, J. N. Chung, C. T. Crowe, and T. R. Troutt, "Particle dispersion by vortex structures in plane mixing layers," J. Fluids Eng. **114**, 657 (1992).
[6]L. Tang, F. Wen, Y. Yang, C. T. Crowe, J. N. Chung, and T. R. Troutt, "Self-organizing particle dispersion mechanism in a plane wake," Phys. Fluids A **4**, 2244 (1992).
[7]K. D. Squires and J. K. Eaton, "Preferential concentration of particles by turbulence," Phys. Fluids A **3**, 1169 (1991).
[8]K. D. Squires and J. K. Eaton, "Particle response and turbulence modification in isotropic turbulence," Phys. Fluids A **2**, 1191 (1990).
[9]S. Elghobashi and G. C. Truesdell, "On the two-way interaction between homogeneous turbulence and dispersed solid particles. I: Turbulence modification," Phys. Fluids A **5**, 1790 (1993).
[10]G. C. Truesdell and S. Elghobashi, "On the two-way interaction between homogeneous turbulence and dispersed solid particles. II. Particle dispersion," Phys. Fluids **6**, 1405 (1994).
[11]M. Boivin, O. Simonin, and K. D. Squires, "Direct numerical simulation of turbulence modulation by particles in isotropic turbulence," J. Fluid Mech. **375**, 235 (1998).
[12]O. A. Druzhinin, "The influence of particle inertia on the two-way coupling and modification of isotropic turbulence by microparticles," Phys. Fluids **13**, 3738 (2001).
[13]A. Ferrante and S. Elghobashi, "On the physical mechanisms of two-way coupling in particle-laden isotropic turbulence," Phys. Fluids **15**, 315 (2003).
[14]M. R. Maxey, "The gravitational settling of aerosol particles in homogeneous turbulence and random flow fields," J. Fluid Mech. **174**, 441 (1987).
[15]L.-P. Wang and M. R. Maxey, "Settling velocity and concentration distribution of heavy particles in homogeneous isotropic turbulence," J. Fluid Mech. **256**, 27 (1993).
[16]R. Mei, "Effect of turbulence on the particle settling velocity in the nonlinear drag range," Int. J. Multiphase Flow **20**, 273 (1994).
[17]C. Y. Yang and U. Lei, "The role of the turbulent scales in the settling velocity of heavy particles in homogeneous isotropic turbulence," J. Fluid Mech. **371**, 179 (1998).
[18]A. Aliseda, A. Cartellier, F. Hainaux, and J. C. Lasheras, "Effect of preferential concentration on the settling velocity of heavy particles in homogeneous isotropic turbulence," J. Fluid Mech. **468**, 77 (2002).
[19]T. S. Yang and S. S. Shy, "The settling velocity of heavy particles in an aqueous near-isotropic turbulence," Phys. Fluids **15**, 868 (2003).
[20]T. S. Yang and S. S. Shy, "Two-way interaction between solid particles and homogeneous air turbulence: particle settling rate and turbulence modification measurements," J. Fluid Mech. **526**, 171 (2005).
[21]V. Eswaran and S. B. Pope, "An examination of forcing in direct numerical simulations of turbulence," Comput. Fluids **16**, 257 (1988).
[22]T. Bosse, C. Härtel, E. Meiburg, and L. Kleiser, "Numerical simulation of finite Reynolds number suspension drops settling under gravity," Phys. Fluids **17**, 037101 (2005).
[23]M. R. Maxey and J. J. Riley, "Equation of motion for a small rigid sphere in a nonuniform flow," Phys. Fluids **26**, 883 (1983).
[24]S. A. Orszag, "Numerical simulation of incompressible flows within simple boundaries: I. Galerkin (spectral) representations," Stud. Appl. Math. **50**, 293 (1971).
[25]S. Elghobashi, "On predicting particle-laden turbulent flows," Appl. Sci. Res. **52**, 309 (1994).
[26]M. R. Maxey and B. K. Patel, "Localized force representations for particles sedimenting in Stokes flow," Int. J. Multiphase Flow **27**, 1603 (2001).
[27]H. Tennekes and J. L. Lumley, *A First Course in Turbulence* (MIT Press, Cambridge, MA, 1972).
[28]S. Schreck and S. J. Kleis, "Modification of grid-generated turbulence by solid particles," J. Fluid Mech. **249**, 665 (1993).
[29]J. D. Kulick, J. R. Fessler, and J. K. Eaton, "Particle response and turbulence modification in fully developed channel flow," J. Fluid Mech. **277**, 109 (1994).
[30]A. Ferrante and S. Elghobashi, "On the physical mechanisms of drag reduction in a spatially developing turbulent boundary layer laden with microbubbles," J. Fluid Mech. **503**, 345 (2004).
[31]S. Sundaram and L. R. Collins, "A numerical study of the modulation of isotropic turbulence by suspended particles," J. Fluid Mech. **379**, 105 (1999).
[32]S. Balachandar and M. R. Maxey, "Methods for evaluating fluid velocities in spectral simulations of turbulence," J. Comput. Phys. **83**, 96 (1989).
[33]P. K. Yeung and S. B. Pope, "An algorithm for tracking fluid particles in numerical simulations of homogeneous turbulence," J. Comput. Phys. **79**, 373 (1988).
[34]S. Sundaram and L. R. Collins, "Numerical considerations in simulating a turbulent suspension of finite-volume particles," J. Comput. Phys. **124**, 337 (1996).